TRE®
Sensing the Planet

# Final Report

## *SqueeSAR™ Analysis of Earl Avenue and Glenview Drive area, San Bruno, California*

**Prepared by:**
**TRE Canada Inc.**
**Doc. Ref.: JO10-3026**
**Confidential**

**February 2, 2011**

**Table of Contents**

# 1 Background

San Bruno is located near the city of San Francisco, California (Figure 1). TRE Canada (TRE) was approached by Pacific Gas and Electric (PG&E) to perform an analysis of ground movement in the Earl Avenue and Glenview Drive area using satellite radar data processed with its proprietary SqueeSAR™ technique. This report contains the results of the analysis.

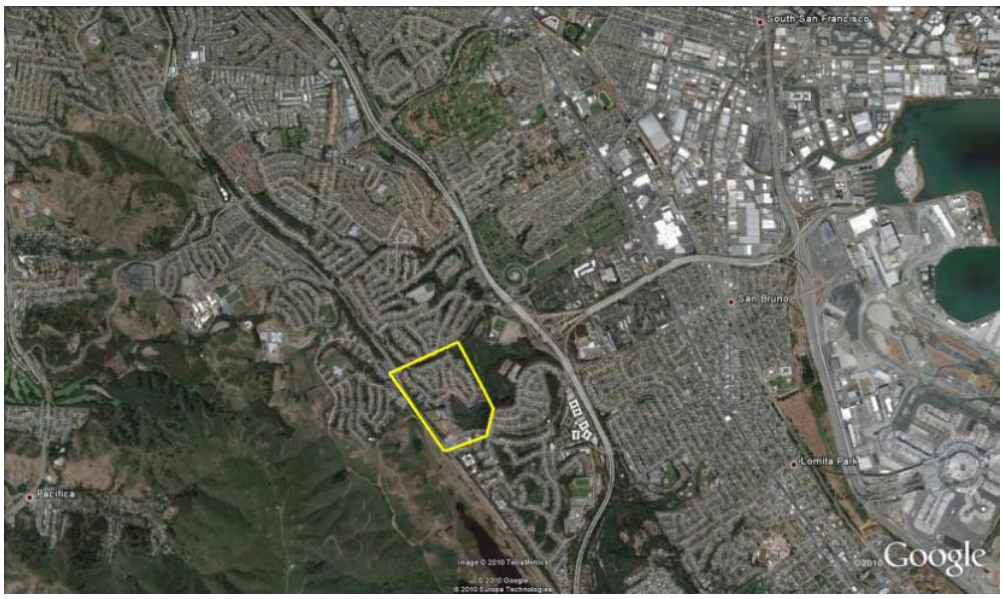


**Figure 1. The location of the area of interest (outlined in yellow) within San Bruno, California as seen on Google Earth.**

# 2 Area of interest and data selection

## 2.1 Area of interest

The area of interest (AOI) is located within the city of San Bruno, California and is approximately 0.22 sq. miles or 0.56 km$^2$ (Figure 2).

Numerous buildings and other man-made structures located throughout the AOI provided excellent stable targets for the SqueeSAR™ analysis. However, no radar targets were identified within a small vegetated area in the southeast portion of the AOI. This was due to the changes in reflectivity that are exhibited by vegetation over time, which causes densely vegetated environments to be unsuitable for most InSAR analyses.

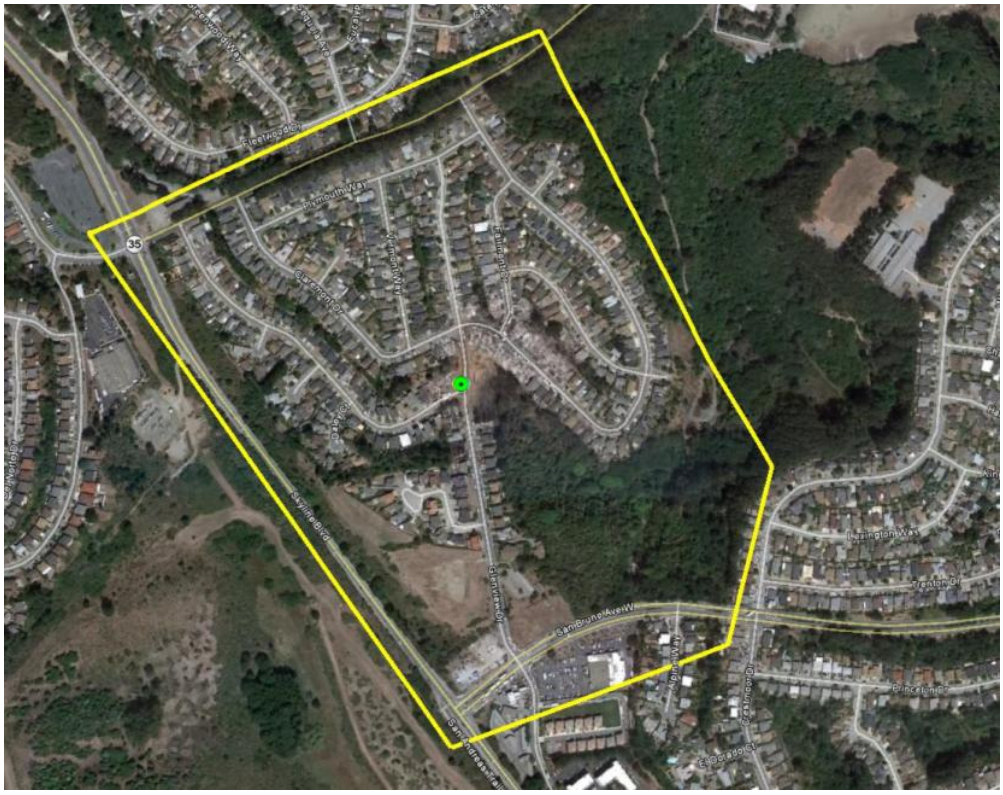

**Figure 2. The extent of the AOI (outlined in yellow) as viewed in Google Earth. The green dot indicates the intersection of Glenview Drive and Earl Avenue.**

## 2.2 Radar data

Four historical datasets were selected for this analysis, including an ESA ERS/1 and ERS/2 descending dataset, a RADARSAT-1 ascending dataset, and ENVISAT ascending and descending datasets.

The first dataset used in this analysis consists of 52 images from the ERS satellite. The satellite images in this dataset were acquired from Frame Number 2853, Track 70 at 2:50:32 AM PST in a descending orbit (satellite traveling from north to south).

The second image archive used for this analysis is from the RADARSAT-1 satellite and comprises a total of 61 scenes. The images were acquired from Track 38 of an ascending orbit with an acquisition start time of 10:30:36 PST (satellite travelling from south to north). No frame number is given, as data is collected continuously along each polar-orbiting track. Individual frames of data are captured by tasking the satellite to acquire an image of set spatial dimension at a specific start time.

The third and fourth datasets are from the ENVISAT satellite and include 46 scenes acquired from an ascending orbit, and a set of 50 images acquired from a descending orbit. The images from the ascending orbit were captured at 1:55:28 PM PST from Frame Number 747, Track 478 and the scenes from the descending orbit were captured at 2:20:33 AM PST from Frame Number 2853, Track 70.

Coverage of the AOI by the satellite imagery datasets are shown in Figure 3 and Figure 4.

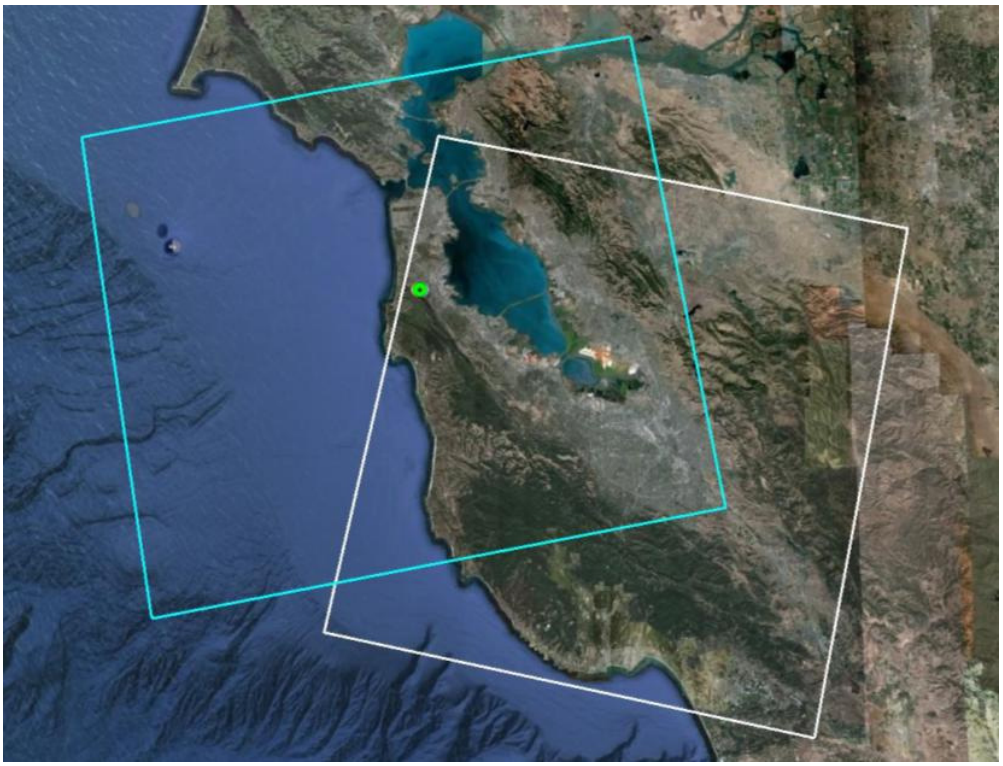

**Figure 3. Coverage of the AOI (indicated by the green dot) by Track 70, Frame Number 2853 of the ERS descending dataset (white outline) and Track 38 of the RADARSAT-1 ascending dataset, with a start time of 10:30:36 PST (blue outline).**

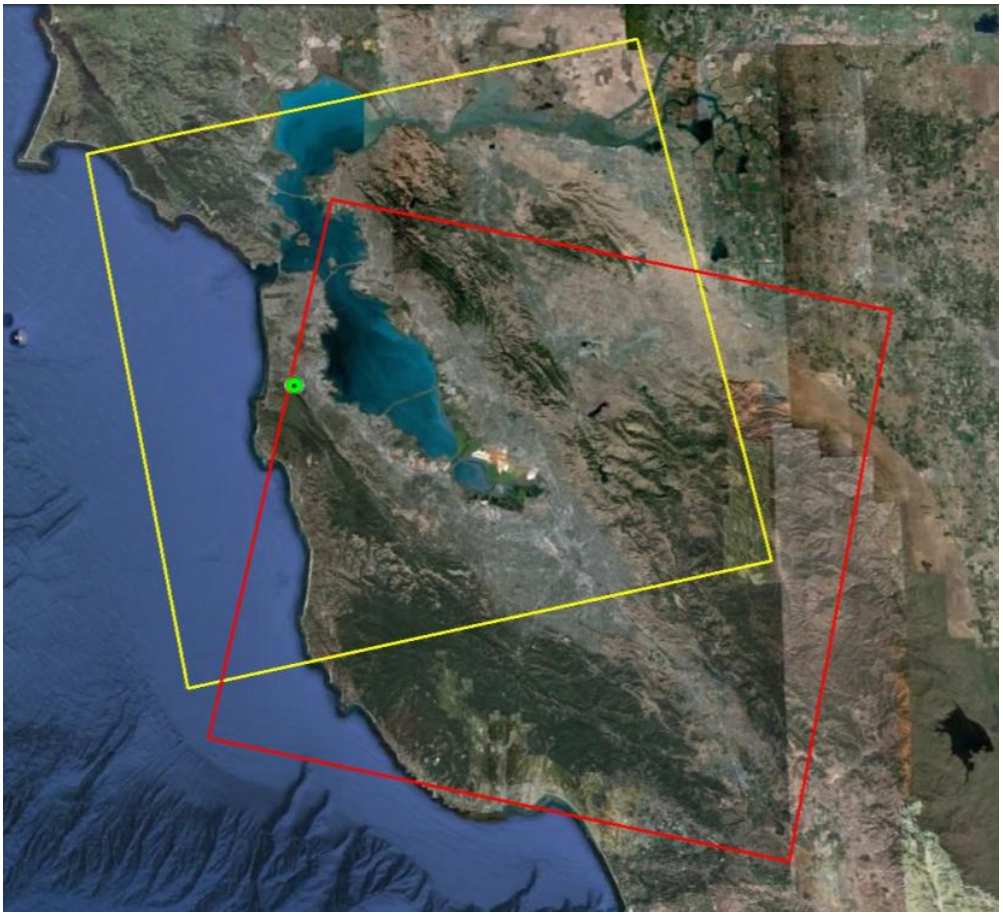

**Figure 4. Coverage of the AOI (indicated by the green dot) by Track 478, Frame Number 747 of the ENVISAT ascending dataset (yellow outline) and Track 70, Frame Number 2853 of the ENVISAT descending (red outline) dataset.**

Table 1 to Table 4 inclusive lists the images for the four datasets used in this analysis. Imagery from the four datasets cover the period from 6 May 1992 to 14 August 2010.

| ID | Date | ID | Date |
|---|---|---|---|
| 1 | 5/6/1992 | 27 | 5/9/1998 |
| 2 | 6/10/1992 | 28 | 7/18/1998 |
| 3 | 7/15/1992 | 29 | 8/22/1998 |
| 4 | 8/19/1992 | 30 | 9/26/1998 |
| 5 | 9/23/1992 | 31 | 10/31/1998 |
| 6 | 1/6/1993 | 32 | 12/5/1998 |
| 7 | 6/30/1993 | 33 | 1/9/1999 |
| 8 | 5/19/1995 | 34 | 2/13/1999 |
| 9 | 9/1/1995 | 35 | 3/20/1999 |
| 10 | 10/7/1995 | 36 | 4/24/1999 |
| 11 | 11/10/1995 | 37 | 5/29/1999 |
| 12 | 11/11/1995 | 38 | 7/3/1999 |
| 13 | 12/15/1995 | 39 | 8/7/1999 |
| 14 | 3/29/1996 | 40 | 9/11/1999 |
| 15 | 3/30/1996 | 41 | 10/16/1999 |
| 16 | 5/3/1996 | 42 | 11/20/1999 |
| 17 | 5/4/1996 | 43 | 12/25/1999 |
| 18 | 8/17/1996 | 44 | 1/29/2000 |
| 19 | 10/26/1996 | 45 | 3/4/2000 |
| 20 | 11/30/1996 | 46 | 4/8/2000 |
| 21 | 1/4/1997 | 47 | 6/17/2000 |
| 22 | 8/2/1997 | 48 | 7/22/2000 |
| 23 | 9/6/1997 | 49 | 8/26/2000 |
| 24 | 10/11/1997 | 50 | 9/30/2000 |
| 25 | 12/20/1997 | 51 | 11/4/2000 |
| 26 | 4/4/1998 | 52 | 12/9/2000 |

**Table 1. Dates of the Track 70, Frame Number 2853 ERS descending images, acquired at 2:50:32 AM PST.**

| ID | Date | ID | Date |
|---|---|---|---|
| 1 | 11/5/2001 | 32 | 4/11/2004 |
| 2 | 11/29/2001 | 33 | 6/22/2004 |
| 3 | 12/23/2001 | 34 | 7/16/2004 |
| 4 | 1/16/2002 | 35 | 8/9/2004 |
| 5 | 3/5/2002 | 36 | 9/2/2004 |
| 6 | 3/29/2002 | 37 | 9/26/2004 |
| 7 | 5/16/2002 | 38 | 11/13/2004 |
| 8 | 6/9/2002 | 39 | 12/7/2004 |
| 9 | 7/3/2002 | 40 | 12/31/2004 |
| 10 | 7/27/2002 | 41 | 1/24/2005 |
| 11 | 8/20/2002 | 42 | 2/17/2005 |
| 12 | 9/13/2002 | 43 | 3/13/2005 |
| 13 | 10/7/2002 | 44 | 4/6/2005 |
| 14 | 10/31/2002 | 45 | 4/30/2005 |
| 15 | 1/11/2003 | 46 | 5/24/2005 |
| 16 | 2/4/2003 | 47 | 6/17/2005 |
| 17 | 2/28/2003 | 48 | 7/11/2005 |
| 18 | 3/24/2003 | 49 | 8/4/2005 |
| 19 | 4/17/2003 | 50 | 8/28/2005 |
| 20 | 5/11/2003 | 51 | 9/21/2005 |
| 21 | 6/4/2003 | 52 | 10/15/2005 |
| 22 | 8/15/2003 | 53 | 12/2/2005 |
| 23 | 9/8/2003 | 54 | 12/26/2005 |
| 24 | 10/2/2003 | 55 | 5/19/2006 |
| 25 | 10/26/2003 | 56 | 6/12/2006 |
| 26 | 11/19/2003 | 57 | 7/30/2006 |
| 27 | 12/13/2003 | 58 | 8/23/2006 |
| 28 | 1/6/2004 | 59 | 12/16/2007 |
| 29 | 1/30/2004 | 60 | 2/2/2008 |
| 30 | 2/23/2004 | 61 | 2/26/2008 |
| 31 | 3/18/2004 | | |

**Table 2. Dates of the RADARSAT-1 ascending images, acquired from Track 38 with a start time of 10:30:36 PST.**

| ID | Date | ID | Date |
|---|---|---|---|
| 1 | 11/3/2002 | 24 | 4/20/2008 |
| 2 | 12/8/2002 | 25 | 5/25/2008 |
| 3 | 2/16/2003 | 26 | 6/29/2008 |
| 4 | 8/10/2003 | 27 | 8/3/2008 |
| 5 | 9/14/2003 | 28 | 9/7/2008 |
| 6 | 10/19/2003 | 29 | 12/21/2008 |
| 7 | 12/28/2003 | 30 | 1/25/2009 |
| 8 | 5/1/2005 | 31 | 3/1/2009 |
| 9 | 6/5/2005 | 32 | 4/5/2009 |
| 10 | 8/14/2005 | 33 | 5/10/2009 |
| 11 | 11/27/2005 | 34 | 6/14/2009 |
| 12 | 5/21/2006 | 35 | 7/19/2009 |
| 13 | 7/30/2006 | 36 | 8/23/2009 |
| 14 | 10/8/2006 | 37 | 9/27/2009 |
| 15 | 11/12/2006 | 38 | 11/1/2009 |
| 16 | 12/17/2006 | 39 | 12/6/2009 |
| 17 | 7/15/2007 | 40 | 1/10/2010 |
| 18 | 8/19/2007 | 41 | 2/14/2010 |
| 19 | 9/23/2007 | 42 | 3/21/2010 |
| 20 | 12/2/2007 | 43 | 4/25/2010 |
| 21 | 1/6/2008 | 44 | 5/30/2010 |
| 22 | 2/10/2008 | 45 | 7/4/2010 |
| 23 | 3/16/2008 | 46 | 8/8/2010 |

**Table 3. Dates of the Track 478, Frame Number 747 ENVISAT ascending images, acquired at 1:55:28 PM PST.**

| ID | Date | ID | Date |
|---|---|---|---|
| 1 | 1/18/2003 | 26 | 3/22/2008 |
| 2 | 9/20/2003 | 27 | 4/26/2008 |
| 3 | 11/29/2003 | 28 | 5/31/2008 |
| 4 | 1/3/2004 | 29 | 7/5/2008 |
| 5 | 2/7/2004 | 30 | 8/9/2008 |
| 6 | 4/17/2004 | 31 | 9/13/2008 |
| 7 | 4/2/2005 | 32 | 10/18/2008 |
| 8 | 5/7/2005 | 33 | 11/22/2008 |
| 9 | 6/11/2005 | 34 | 1/31/2009 |
| 10 | 2/11/2006 | 35 | 3/7/2009 |
| 11 | 3/18/2006 | 36 | 4/11/2009 |
| 12 | 4/22/2006 | 37 | 5/16/2009 |
| 13 | 5/27/2006 | 38 | 6/20/2009 |
| 14 | 7/1/2006 | 39 | 7/25/2009 |
| 15 | 8/5/2006 | 40 | 8/29/2009 |
| 16 | 10/14/2006 | 41 | 10/3/2009 |
| 17 | 11/18/2006 | 42 | 11/7/2009 |
| 18 | 12/23/2006 | 43 | 12/12/2009 |
| 19 | 7/21/2007 | 44 | 1/16/2010 |
| 20 | 8/25/2007 | 45 | 2/20/2010 |
| 21 | 9/29/2007 | 46 | 3/27/2010 |
| 22 | 11/3/2007 | 47 | 5/1/2010 |
| 23 | 12/8/2007 | 48 | 6/5/2010 |
| 24 | 1/12/2008 | 49 | 7/10/2010 |
| 25 | 2/16/2008 | 50 | 8/14/2010 |

**Table 4. Dates of the Track 70, Frame Number 2853 ENVISAT descending images, acquired at 2:20:33 AM PST.**

# 3 Results of the SqueeSAR™ analysis

## 3.1 Reference point

SqueeSAR™ is a differential technique: displacement is measured compared to a reference point that is assumed to be stable.

Each of the four datasets has a reference point. The reference points were selected as close together as possible within an area deemed to be stable by Exponent-Failure Analysis Associates, Inc. (Exponent), to ensure comparability of the displacement rates measured by the four datasets. The locations of the four reference points for San Bruno are shown in Figure 5 and Figure 6. The exact coordinates of the four reference points are provided in Table 5 to Table 8.

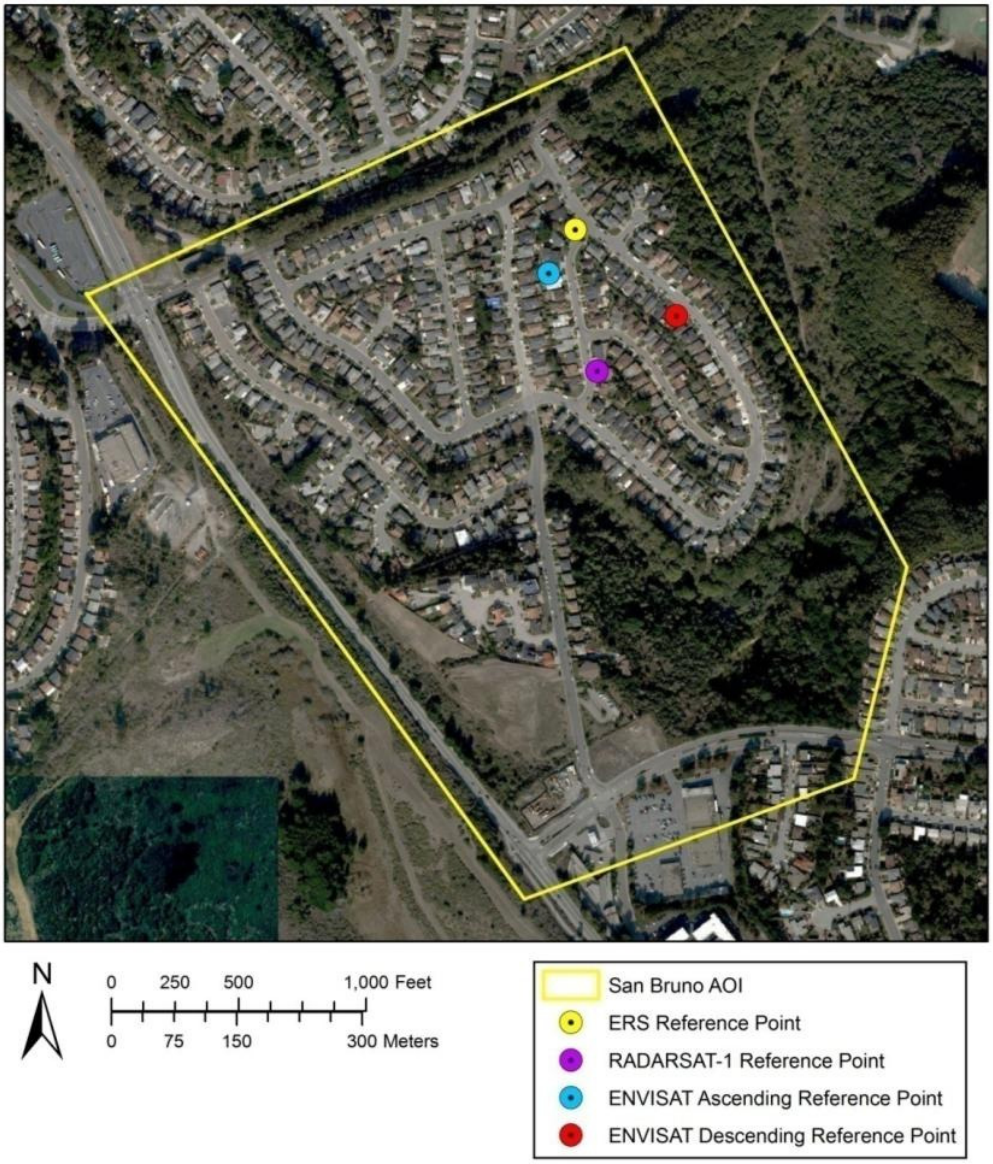


**Figure 5. The locations of the reference points used in the analysis of the four datasets.**


**Figure 6. A close-up of the reference points used in the analysis of the four datasets.**

## 3.2 Displacement rate

Figure 7 shows the displacement rate of the Permanent Scatterers (PS), expressed in mm/yr, as identified in the SqueeSAR™ analysis of the four datasets. The average velocity is calculated from the linear regression of the time series. PS are color-coded according to their annual rate of movement.

Negative velocities indicate downward movement and positive velocities indicate upward movement relative to the satellites line of sight as discussed in Section 7.

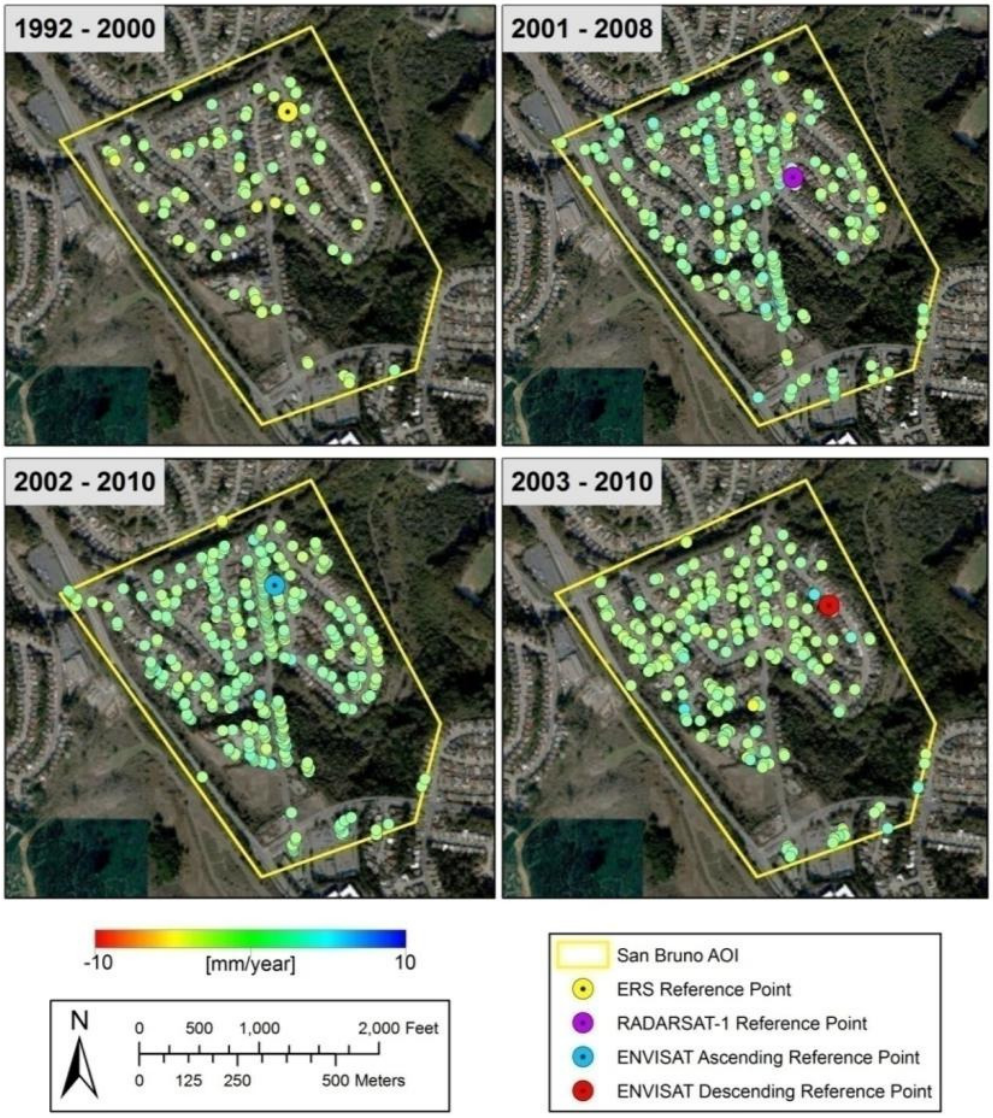


**Figure 7. PS displacement rates derived from the SqueeSAR™ analysis of the ERS descending (top left), RADARSAT-1 ascending (top right), ENVISAT ascending (bottom left) and ENVISAT descending (bottom right) datasets.**

A displacement time series is also provided for each scatterer. Figure 8 shows the Permanent Scatterers identified from the ENVISAT ascending dataset near the intersection of Earl Avenue and Glenview Drive. Ground displacement measured at the indicated PS is shown in Figure 9.

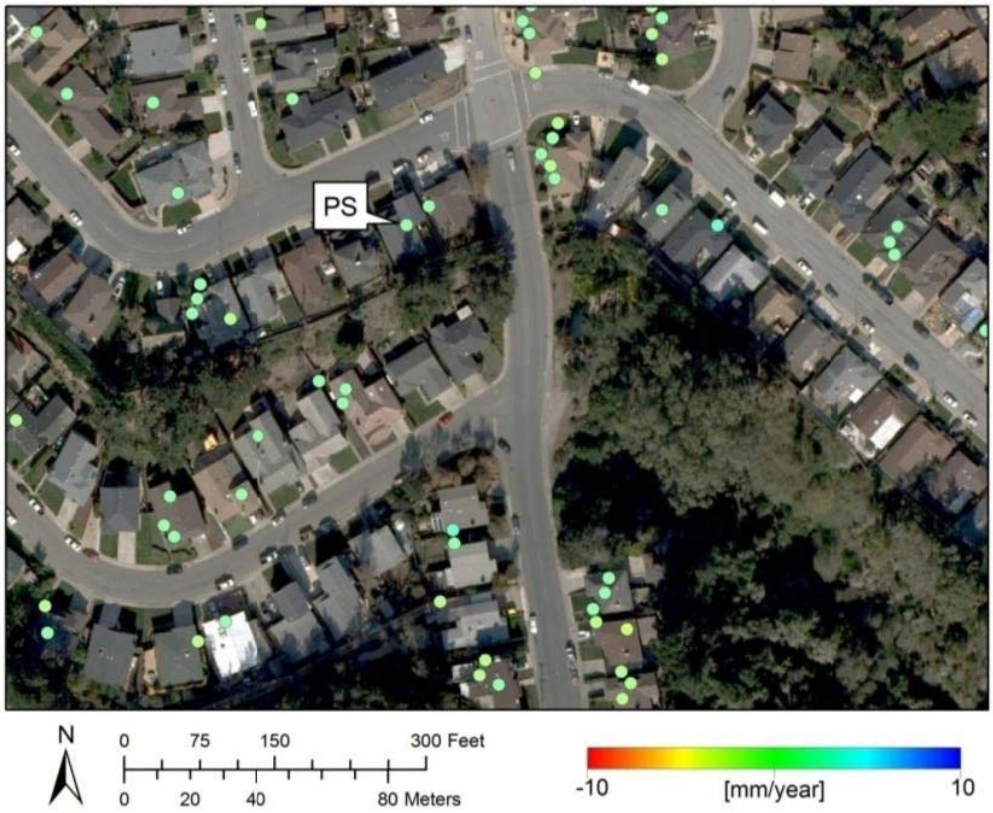


**Figure 8. A close-up of PS displacement rates derived from the SqueeSAR™ analysis of the ENVISAT ascending dataset over the Earl Avenue and Glenview Drive area. A time series of the point labelled PS is shown in Figure 9.**

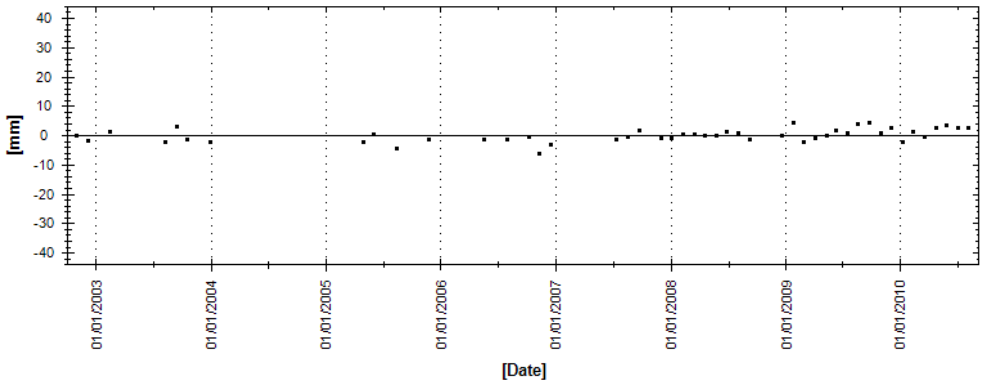


**Figure 9. Time series (ground displacement measured between 3 November 2002 and 8 August, 2010) for the point labelled PS in Figure 8.**

Figure 10 shows the displacement rate of the Distributed Scatterers (DS), expressed in mm/yr, as identified in the SqueeSAR™ analysis of the four datasets. DS are color-coded according to their annual rate of movement. A displacement time series is also provided for each DS.

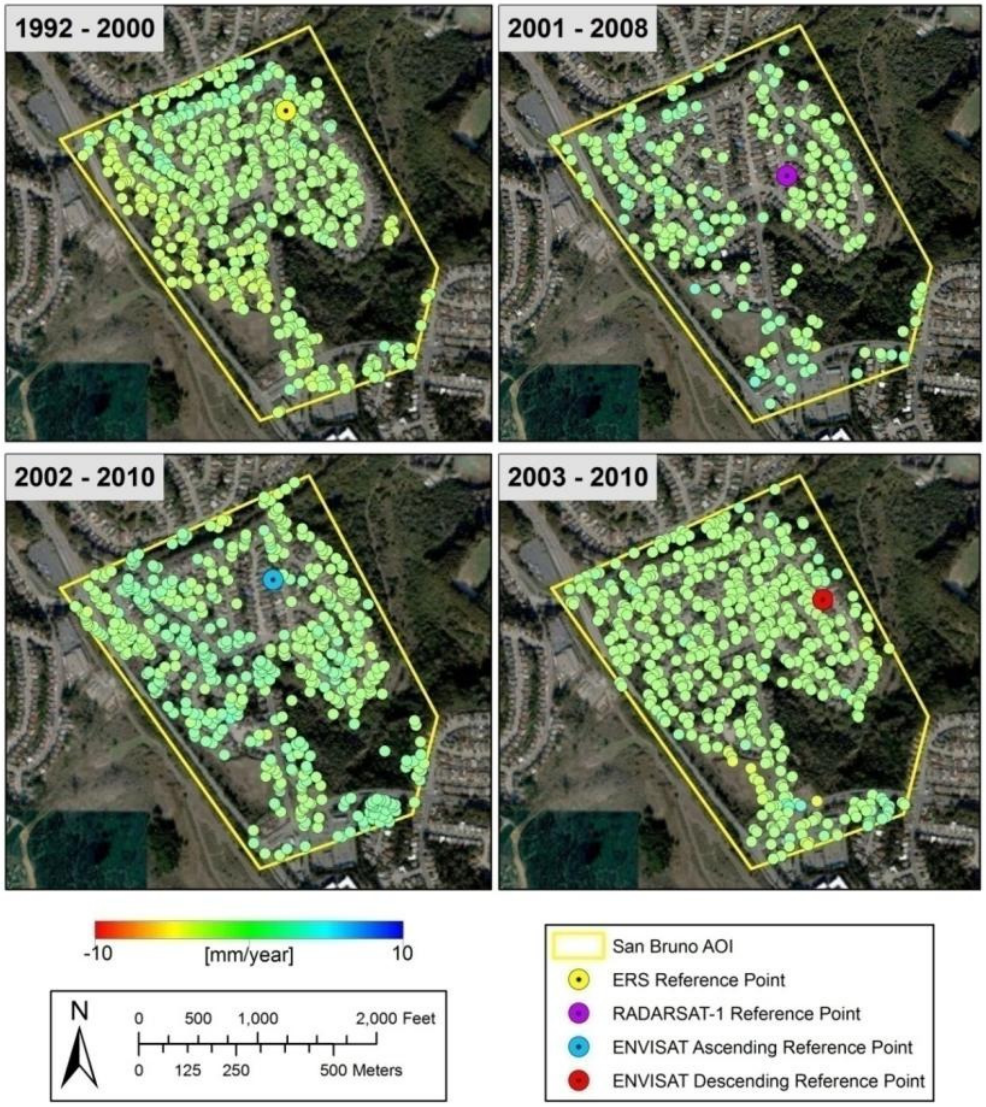


**Figure 10. DS displacement rates derived from the SqueeSAR™ analysis of the ERS descending (top left), RADARSAT-1 ascending (top right), ENVISAT ascending (bottom left) and ENVISAT descending (bottom right) datasets.**

It is important to note that Distributed Scatterers (DS) represent homogeneous and contiguous areas of reflectivity rather than individual points or features. The purpose of representing the DS as points in Figure 10 is for clarity of presentation.

Figure 11 provides all Distributed Scatterers within the AOI, symbolized by a square corresponding to the area of each DS. The square symbols used in Figure 11 represent DS size only, and do not correspond to the true shape/extent of the DS.

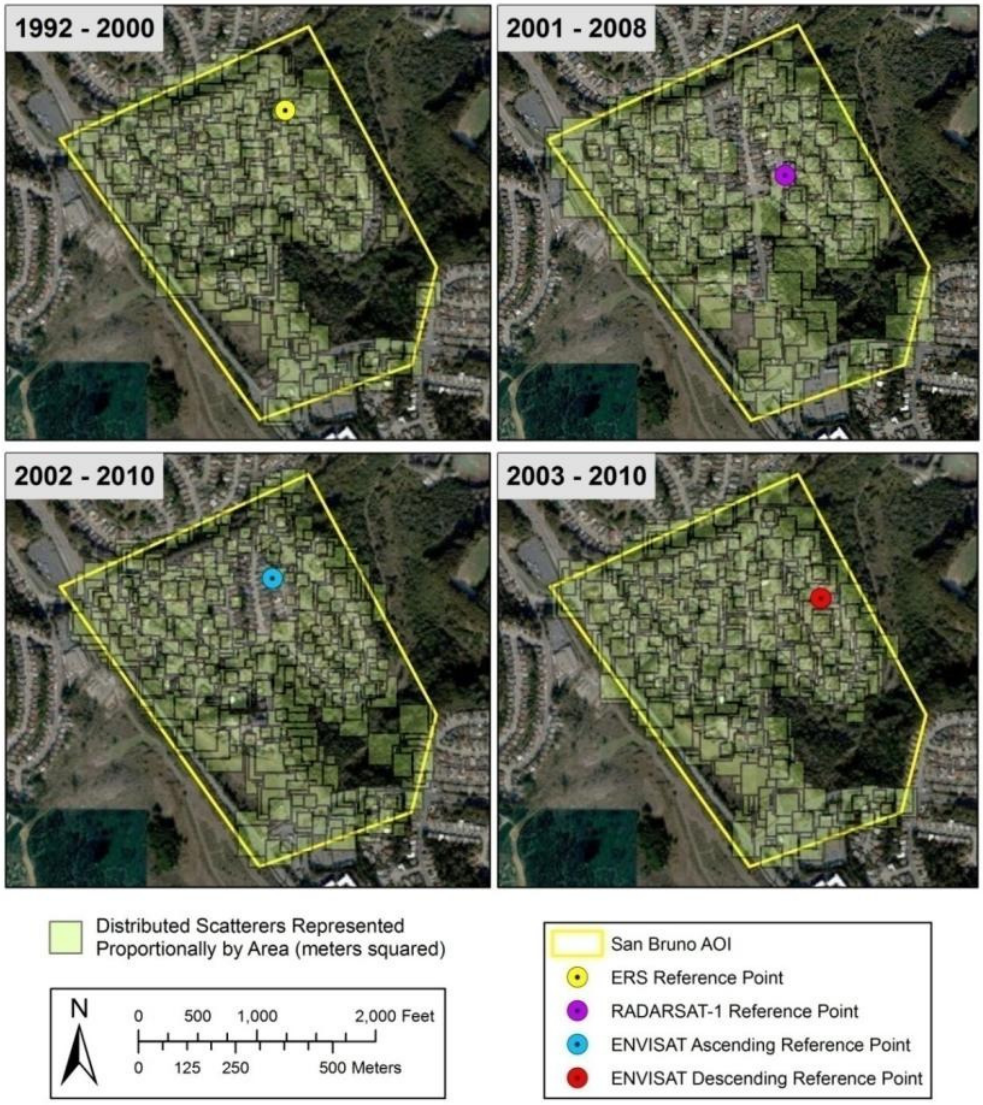


**Figure 11. DS identified in the ERS descending (top left), RADARSAT-1 ascending (top right), ENVISAT ascending (bottom left) and ENVISAT descending (bottom right) datasets, represented proportionally by the area they cover. Note that the true shape of DS are not represented.**

## 3.3 Acceleration

PS and DS acceleration values (Figure 12) can be used to identify non-linear trends in the time series.

Negative accelerations are marked in red and indicate either an increase in downward movement rates or a decrease in uplift. Positive accelerations are blue and indicate either an increase in the rate of uplift or a decrease in the rate of subsidence.

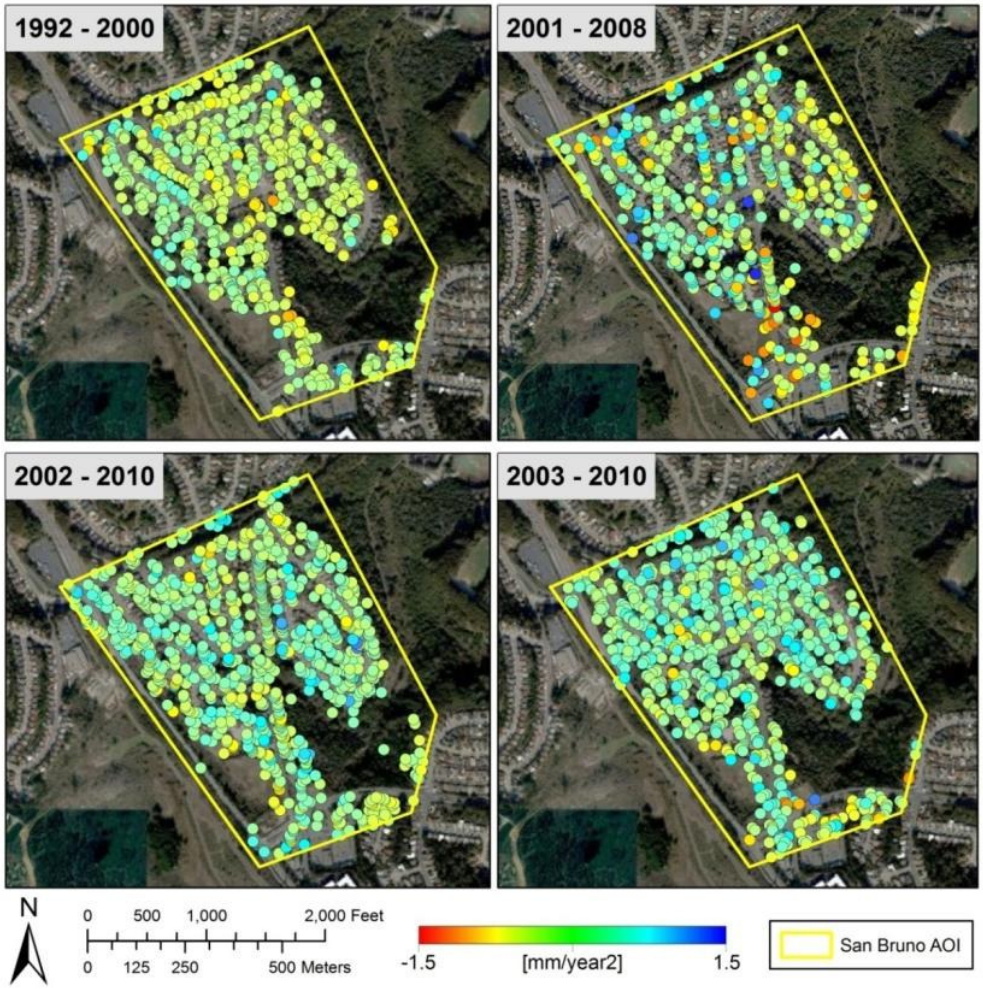


**Figure 12. PS and DS acceleration, in mm/yr$^2$ for the ERS descending (top left), RADARSAT-1 ascending (top right), ENVISAT ascending (bottom left) and ENVISAT descending (bottom right) datasets.**

## 3.4 Seasonal amplitude

The seasonal amplitude map represents cyclical (seasonal) trends that are present in the deformation rate (Figure 13). PS and DS displacement data are fitted to a sinusoidal model to characterize the range of displacement values measured at each point. The seasonal amplitude value represents the average range of upward and downward ground movement measured for each year of analysis.

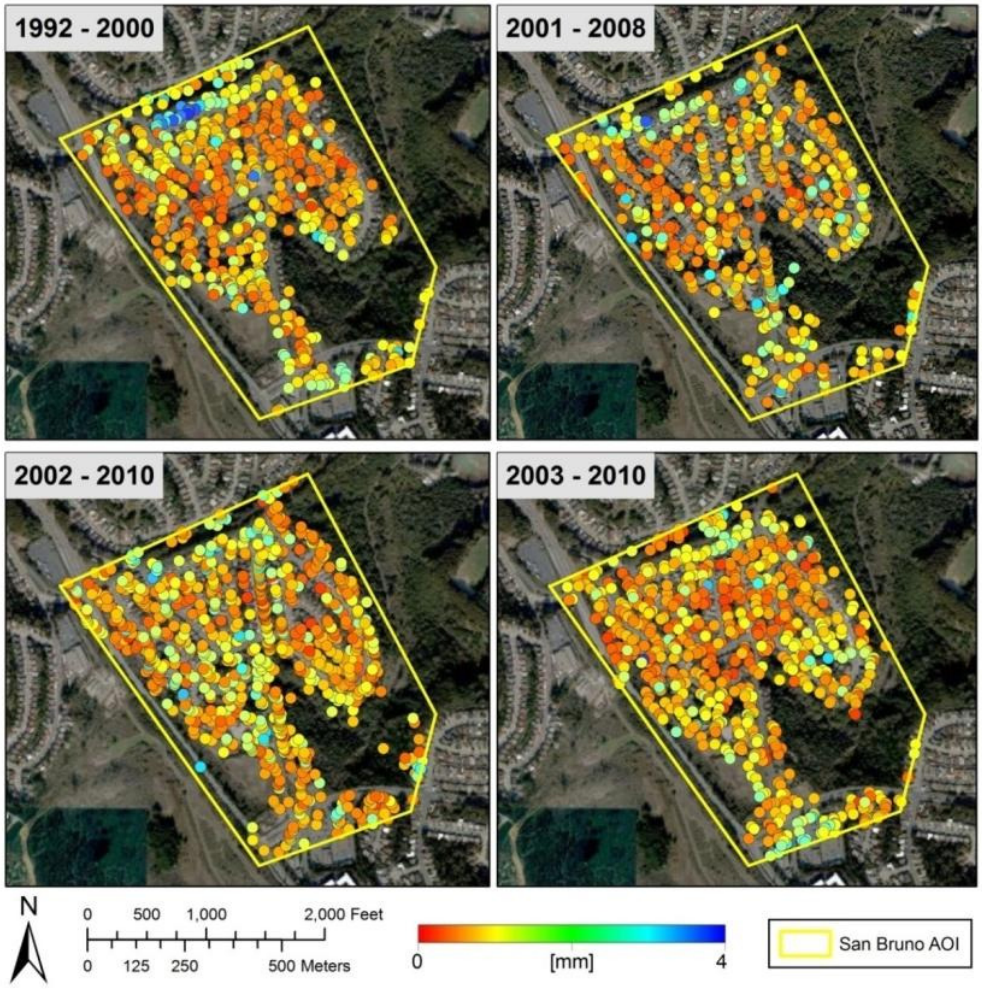


**Figure 13. PS and DS seasonal amplitude, in mm for the ERS descending (top left), RADARSAT-1 ascending (top right), ENVISAT ascending (bottom left) and ENVISAT descending (bottom right) datasets.**

## 3.5 Other Properties of the Data

Table 6 to Table 8 inclusive (below), provides a summary of the other properties relative to the data processing.

| | |
|---|---|
| **Satellite** | ERS |
| **Acquisition geometry** | Descending |
| **Critical baseline [m]** | 1286.8605 |
| **Pixel Resolution [m]** | 20x4 |
| **Analysis time interval** | 5/6/1992 - 12/9/2000 |
| **Time of Day Image Acquired** | 2:50:32 AM PST |
| **Number of scenes processed** | 52 |
| **Georeferencing** | PS aligned on Microsoft Virtual Earth |
| **Projection system used / datum** | NAD_1983_UTM_Zone_10N |
| **Reference Point location** | North: 4164372.0508, East: 549296.8093 |
| **Number of PS + DS identified**<br>- **Number of PS**<br>- **Number of DS** | 631<br>89<br>542 |
| **Number of Time Series** | 630 |
| **Average PS + DS density** | 2868 PS and DS per sq. mi.<br>(1127 PS and DS per $km^2$) |

**Table 5. Statistics of the processed data for the ERS descending image archive.**

| | |
|---|---|
| **Satellite** | RADARSAT-1 |
| **Acquisition geometry** | Ascending |
| **Critical baseline [m]** | 1824.9676 |
| **Pixel Resolution [m]** | 20x5 |
| **Date Range of Imagery** | 11/5/2001 - 2/26/2008 |
| **Time of Day Image Acquired** | 10:30:36 AM PST |
| **Number of scenes processed** | 61 |
| **Georeferencing** | PS aligned on Microsoft Virtual Earth |
| **Projection system used / datum** | NAD_1983_UTM_Zone_10N |
| **Reference Point location** | North:4164202.4401, East: 549323.0517 |
| **Number of PS + DS identified**<br>- **Number of PS**<br>- **Number of DS** | 522<br>279<br>243 |
| **Number of Time Series** | 521 |
| **Average PS + DS density** | 2373 PS and DS per sq. mi.<br>(932 PS and DS per $km^2$) |

**Table 6: Statistics of the processed data for the RADARSAT-1 ascending image archive.**

| | |
|---|---|
| **Satellite** | ENVISAT |
| **Acquisition geometry** | Ascending |
| **Critical baseline [m]** | 1095.8049 |
| **Pixel Resolution [m]** | 20x4 |
| **Analysis time interval** | 11/3/2002 - 8/8/2010 |
| **Time of Day Image Acquired** | 1:55:28 PM PST |
| **Number of scenes processed** | 46 |
| **Georeferencing** | PS aligned on Microsoft Virtual Earth |
| **Projection system used / datum** | NAD_1983_UTM_Zone_10N |
| **Reference Point location** | North: 4164319.5058, East: 549264.9815 |
| **Number of PS + DS identified**<br>- **Number of PS**<br>- **Number of DS** | 870<br>358<br>512 |
| **Number of Time Series** | 869 |
| **Average PS + DS density** | 3955 PS and DS per sq. mi.<br>(1554 PS and DS per $km^2$) |

**Table 7. Statistics of the processed data for the ENVISAT ascending image archive.**

| | |
|---|---|
| **Satellite** | ENVISAT |
| **Acquisition geometry** | Descending |
| **Critical baseline [m]** | 1095.8049 |
| **Pixel Resolution [m]** | 20x4 |
| **Analysis time interval** | 1/18/2003 - 8/14/2010 |
| **Time of Day Image Acquired** | 2:20:33 AM PST |
| **Number of scenes processed** | 50 |
| **Georeferencing** | PS aligned on Microsoft Virtual Earth |
| **Projection system used / datum** | NAD_1983_UTM_Zone_10N |
| **Reference Point location** | North: 4164268.9683, East: 549417.7405 |
| **Number of PS + DS identified**<br>- **Number of PS**<br>- **Number of DS** | 784<br>244<br>540 |
| **Number of Time Series** | 783 |
| **Average PS + DS density** | 3564 PS and DS per sq. mi.<br>(1400 PS and DS per $km^2$) |

**Table 8. Statistics of the processed data for the ENVISAT descending image archive.**

The critical baseline is the maximum admissible separation distance between satellite orbits for an InSAR analysis. Interferometry cannot be performed if the orbits are separated by more than this distance.

# 4 Delivery of Data

The deliverables of the SqueeSAR™ analysis include the present report, the PS and DS data files and a software tool for assisting with the loading, viewing and interrogation of the data in ESRI ArcGIS 9.x software. Table 9 lists all the files contained on the accompanying CD.

| File name | Description |
|---|---|
| SAN_BRUNO_ERS_D_T70_2853_PS_ONLY-TSR.dbf<br>SAN_BRUNO_RSAT_S3_A_T38_PS_ONLY-TSR.dbf<br>SAN_BRUNO_ENVS2_V_A_T478_PS_ONLY-TSR.dbf<br>SAN_BRUNO_ENVS2_V_D_T70_PS_ONLY-TSR.dbf | Tables containing the height, velocity, velocity standard deviation, acceleration, coherence and time series of all the PS identified in the analysis of the four datasets. |
| SAN_BRUNO_ERS_D_T70_2853_PS_ONLY-TSR.shp<br>SAN_BRUNO_RSAT_S3_A_T38_PS_ONLY-TSR.shp<br>SAN_BRUNO_ENVS2_V_A_T478_PS_ONLY-TSR.shp<br>SAN_BRUNO_ENVS2_V_D_T70_PS_ONLY-TSR.shp | ESRI Shapefiles for displaying the database (dbf) files in a GIS environment. |
| SAN_BRUNO_ERS_D_T70_2853_DS_ONLY-TSR.dbf<br>SAN_BRUNO_RSAT_S3_A_T38_DS_ONLY-TSR.dbf<br>SAN_BRUNO_ENVS2_V_A_T478_DS_ONLY-TSR.dbf<br>SAN_BRUNO_ENVS2_V_D_T70_DS_ONLY-TSR.dbf | Tables containing the height, velocity, velocity standard deviation, acceleration, coherence and time series of all the DS identified in the analysis of the four datasets. |
| SAN_BRUNO_ERS_D_T70_2853_DS_ONLY-TSR.shp<br>SAN_BRUNO_RSAT_S3_A_T38_DS_ONLY-TSR.shp<br>SAN_BRUNO_ENVS2_V_A_T478_DS_ONLY-TSR.shp<br>SAN_BRUNO_ENVS2_V_D_T70_DS_ONLY-TSR.shp | ESRI Shapefiles for displaying the database (dbf) files in a GIS environment. |
| SAN_BRUNO_ERS_D_T70_2853-REF.dbf<br>SAN_BRUNO_RSAT_S3_A_T38-REF.dbf<br>SAN_BRUNO_ENVS2_V_A_T478-REF.dbf<br>SAN_BRUNO_ENVS2_V_D_T70-REF.dbf | The reference point s used to process the four datasets. |
| SAN_BRUNO_ERS_D_T70_2853-REF.shp<br>SAN_BRUNO_RSAT_S3_A_T38 -REF.shp<br>SAN_BRUNO_ENVS2_V_A_T478-REF.shp<br>SAN_BRUNO_ENVS2_V_D_T70-REF.shp | ESRI Shapefiles for displaying the reference point files in a GIS environment. |
| San_Bruno_AOI_UTM.shp | Shapefile of the AOI. |
| San_Bruno.mxd | ESRI ArcGIS 9.3 project containing all PS data and the AOI shapefile. |
| TRE3_EndUserLicence.pdf | End User License. |
| TreCustomerToolbarSetup_1.0.8.exe | Installer of the PS tool for ESRI ArcGIS 9.x. |

**Table 9. List of delivered files.**

The ESRI ArcGIS 9.x project file is included to make it easier to view the data. Once the data contained in the CD has been saved to the user's hard drive it will be sufficient to open the project file with ArcGIS and update the links to indicate the locations of the new data.

# 5 The structure of the DBF files

Table 10 shown below, describes the attributes of each PS and DS within the database.

| Field | Description |
|---|---|
| **CODE** | Unique identification code. |
| **SHAPE** | Indicates type of geometry (point). |
| **HEIGHT** [m] | Elevation above sea level of the PS and DS. |
| **H_STDEV** [m] | Standard deviation of PS and DS elevation value. |
| **VEL** [mm/yr] | PS movement rate. Positive values correspond to acceleration *toward the satellite (uplift);* negative values correspond to motion *away from the satellite (subsidence)*. |
| **V_STDEV** [mm/yr] | Standard deviation of PS and DS displacement rate. |
| **ACC** [mm/yr$^2$] | PS and DS Acceleration. |
| **A_STDEV** [mm/yr$^2$] | Standard deviation of PS and DS acceleration value. |
| **COHERENCE** | Quality measure [between 0 and 1]. |
| **SEASON_AMP** [mm] | Amplitude of seasonal cycles present within the data. |
| **SEASON_PHS** [days] | Phase of seasonal cycles present within the data. |
| **S_AMP_STD** [mm] | Standard deviation of the seasonal amplitude. |
| **S_PHS_STD** [days] | Standard deviation of the seasonal phase. |
| **EFF_AREA** [m$^2$] | Size of the area belonging to the PS and DS. For PS EFF_AREA = 0, for DS EFF_AREA > 0. |
| **SRTMERR** [m] | Error to the SRTM (Shuttle Radar Topography Mission) Digital Elevation Model. |
| **D(year/month/day)** [mm] | Following the SRTMERR column are a series of fields that contain the displacement values of successive acquisitions relative to the Master, expressed in mm. |

**Table 10: Description of the fields contained in the Shapefiles.**

# 6 Precision Assessment

Three parameters are used to characterize the PS results:

- Precision of the estimated displacement results;
- Precision of the estimated elevations;
- Precision of the geocoding.

The typical precision of measured displacement rates obtained from the SqueeSAR™ analysis of ERS, RADARSAT-1, and ENVISAT satellite imagery is <1mm/year for all radar targets located within 1 km of the reference point and estimated from a dataset containing 45 SAR acquisitions or more. If the displacement measured between two contiguous satellite images is considered, the accuracy of this single measurement is $\pm$5 mm when the radar target is located within 1 km from the reference point and processed using a dataset containing more than 45 scenes. All of the radar data in the area of interest described in this report are within 1 km of the reference point and were derived from datasets greater than 45 scenes.

Positional (elevation and geocoding) errors are determined by the resolution of the SAR system in use. The imagery from the ERS and ENVISAT satellites used in this analysis both have a cell size of 20 m in the *range* direction (east-west) and 4 m in the *azimuth* direction (north-south direction). The imagery from the RADARSAT-1 satellite used in this analysis has a range resolution of 20 m and an azimuth resolution of 5 m. For data of this resolution, geocoding accuracy generally equals ±6 m in *range* direction, ±2 m in *azimuth* direction and ±1.5 m in elevation (height) for all points located within 1 km of the reference point and estimated from a dataset with at least 45 scenes. Again, all of the radar data in the area of interest described in this report are within 1 km of the reference point and were derived from datasets greater than 45 scenes.

## 6.1 Precision of the Results

The most important factors impacting data precision are:

- Spatial density of the PS (the lower the density, the higher the error)
- Quality of the radar targets (signal-to-noise ratio levels)
- Climatic conditions at the time of the acquisitions
- Distance between the measurement point and the reference

The precision of the data (one standard deviation) is shown in Figure 14. Standard deviation values of the estimated displacement rates are a function of the factors listed above and of local ground movement dynamics.

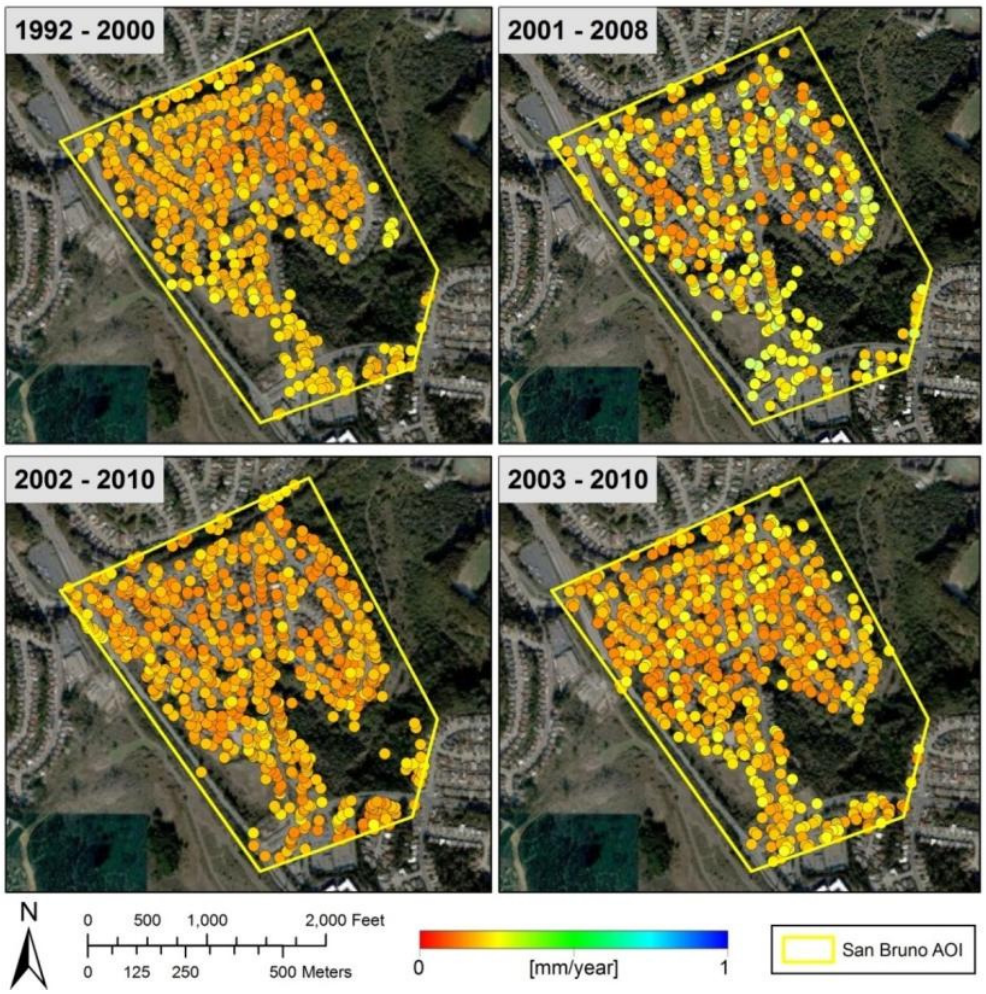


**Figure 14. Standard deviation of the velocity values calculated from the SqueeSAR™ processing of the ERS descending (top left), RADARSAT-1 ascending (top right), ENVISAT ascending (bottom left) and ENVISAT descending (bottom right) datasets.**

# 7 Sensitivity Versors

In all InSAR analyses the displacement measurements are one-dimensional and are carried out along the satellite line-of-sight (LOS). The LOS angle varies depending on the satellite and on the acquisition parameters. Another important parameter is the angle the satellite orbit forms with the geographic North.

Acquisition geometries for the four datasets are shown in Figure 15 and Figure 16. The symbol δ (delta) represents the LOS angle and Θ (theta) the angle with the North. Table 11 contains the values of the angles for this study.

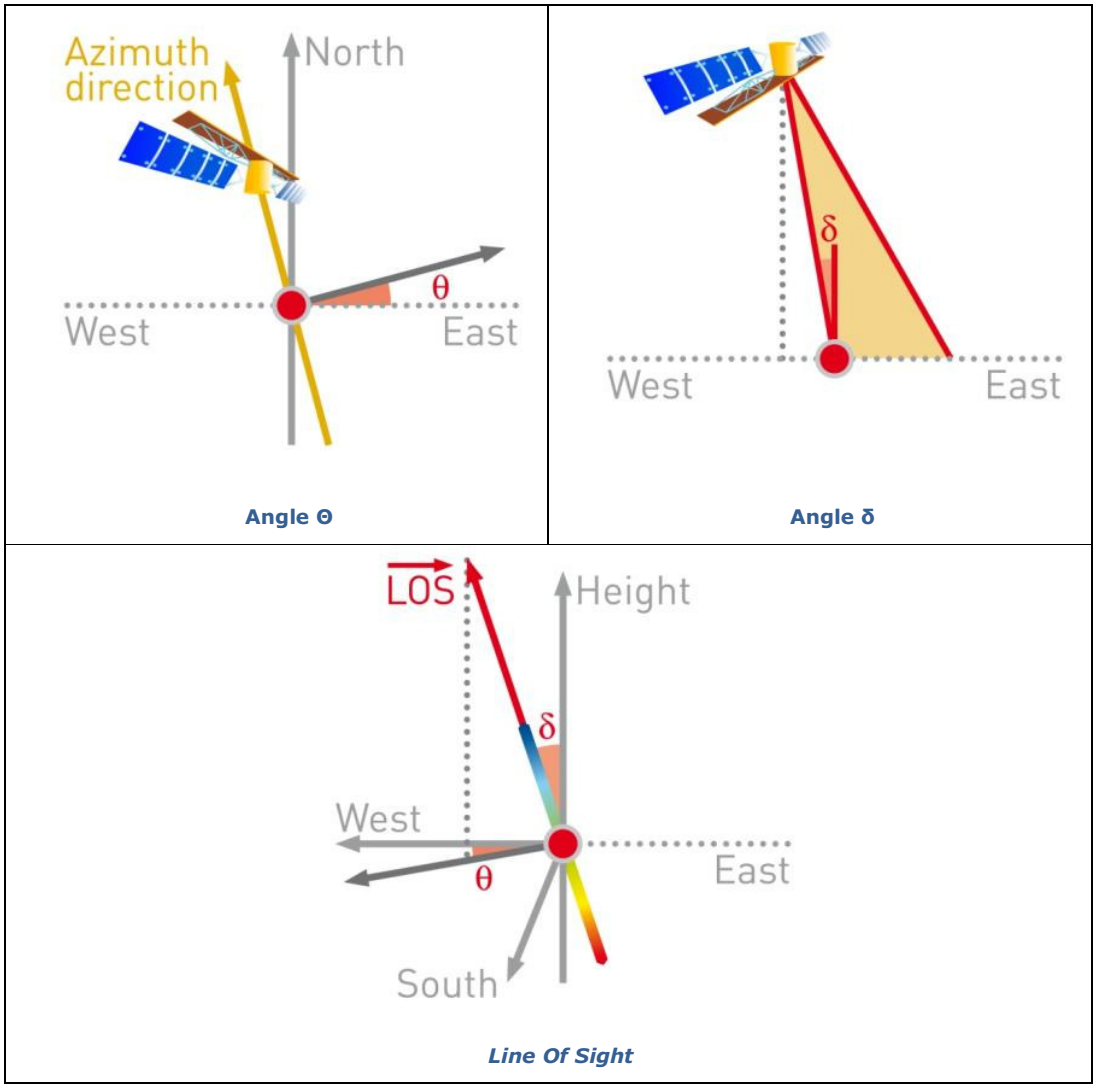


**Figure 15. Diagram illustrating the satellite acquisition geometry for the ascending datasets used in this analysis (RADARSAT-1 and ENVISAT ascending). See Table 11 for the value of the angles.**

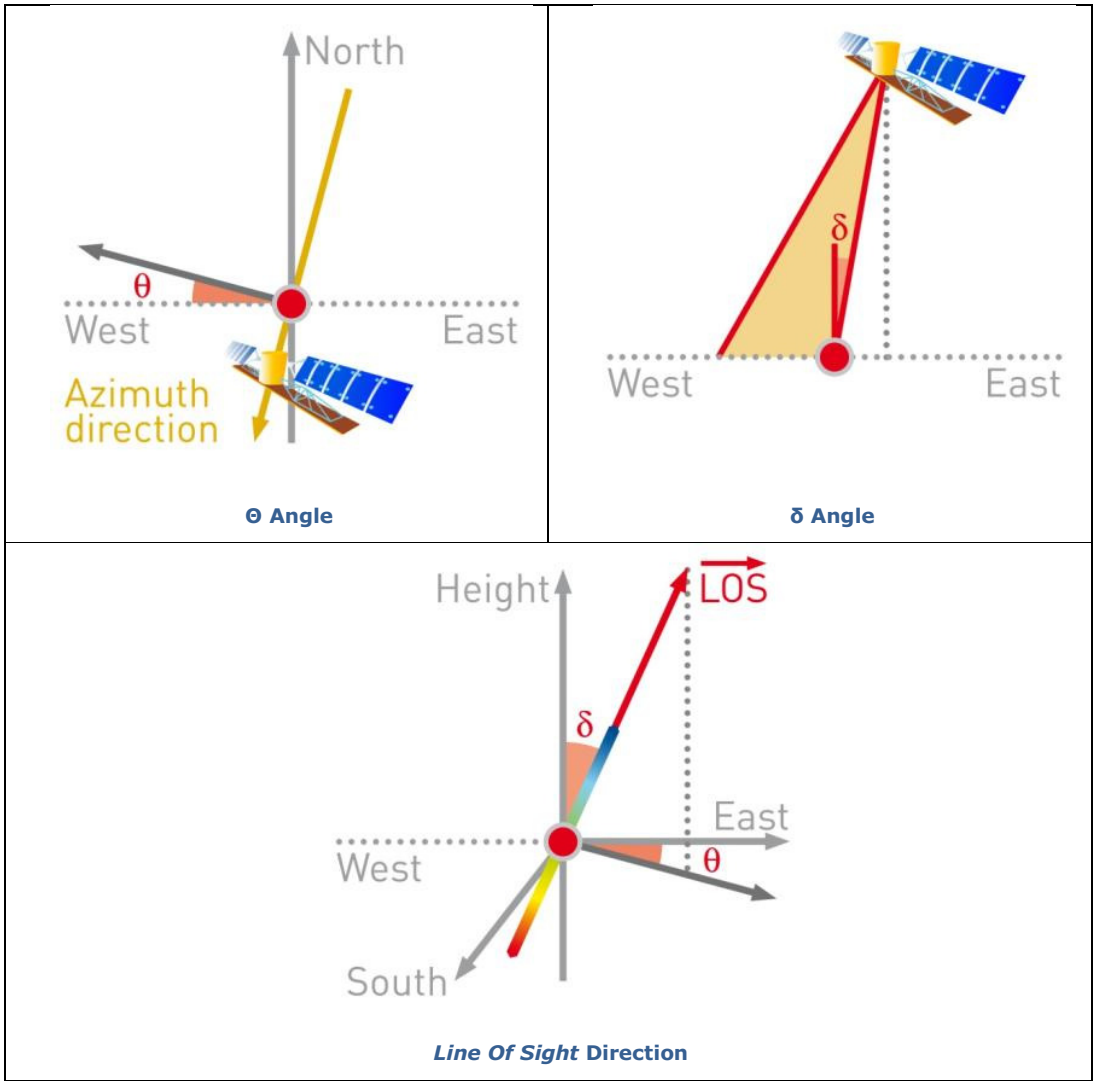


**Θ Angle**

**δ Angle**

***Line Of Sight* Direction**

**Figure 16. Diagram illustrating the satellite acquisition geometry for the descending datasets used in this analysis (ENVISAT and ERS descending). See Table 11 for the value of the angles.**

| Dataset | Orbit geometry | Symbol | Angle |
|---|---|---|---|
| **ERS** | **Descending** | **δ** | 25.98 |
| | | **θ** | 11.40 |
| **RADARSAT-1** | **Ascending** | **δ** | 34.31 |
| | | **θ** | 11.16 |
| **ENVISAT** | **Ascending** | **δ** | 20.92 |
| | | **θ** | 12.64 |
| **ENVISAT** | **Descending** | **δ** | 26.11 |
| | | **θ** | 11.41 |

**Table 11. Satellite viewing angles for the four radar imagery datasets.**

Table 12 contains the LOS versor properties for the present study. These values can be used to determine the sensitivity of the LOS to the vertical, East and North directions. As an example, consider the 34.31 off-nadir viewing angle of the RADARSAT-1 historical dataset. It is quite steep and gives rise to a versor value of 0.826 (obtained as the cosine of δ). This implies that the sensor is very sensitive to vertical motion. Conversely, the sensitivity to movement in the East-West direction is somewhat lower (-0.553) and to the North-South direction sensitivity is lower yet (-0.109).

| Dataset | Direction | Component of the versor |
|---|---|---|
| **ERS** | **North** | -0.08660 |
| | **East** | 0.42937 |
| | **Vertical** | 0.89897 |
| **RADARSAT-1** | **North** | -0.10913 |
| | **East** | -0.55300 |
| | **Vertical** | 0.82600 |
| **ENVISAT Ascending** | **North** | -0.07815 |
| | **East** | -0.34840 |
| | **Vertical** | 0.93408 |
| **ENVISAT Descending** | **North** | -0.08706 |
| | **East** | 0.43147 |
| | **Vertical** | 0.89792 |

**Table 12. Components of the LOS versor for this study.**

# Appendix 1: Radar Interferometry

## InSAR

Interferometric Synthetic Aperture Radar, also referred to as SAR interferometry or InSAR, is the measurement of signal phase change (interference) between radar images. When a point on the ground moves, the distance between the sensor and the point changes, thereby producing a corresponding shift in signal phase. This shift is used to quantify the ground movement.

An interferogram is a 2D representation of the difference in phase values. Variations of phase in an interferogram are identified by fringes, colored bands that indicate areas where and how much movement is occurring. The precision with which the movement can be measured is usually in the centimeter range as the phase shift is also impacted by topographic distortions, atmospheric effects, and other sources of noise.

## DInSAR

When InSAR is used to identify and quantify ground movement, the process is referred to as Differential InSAR (DInSAR). In DInSAR topographic effects are removed by using a DEM of the area of interest to create a differential interferogram.

DInSAR is still impacted by atmospheric effects, as there is no method for removing this signal phase contribution. It is a useful tool for identifying footprints of progressing movement and creating deformation maps. The limitations of DInSAR are its relatively low precision (centimeter scale) and that it cannot distinguish between linear and non-linear motion.

## PSInSAR™

PSInSAR™ is an advanced form of DInSAR. The fundamental difference is that it uses multiple interferograms created from a stack of at least 15 radar images.

PSInSAR™ was developed to overcome the errors produced by atmospheric artefacts on signal phase. The PSInSAR™ algorithm automatically searches the interferograms for pixels that display stable radar reflectivity characteristics throughout every image of the dataset. In PSInSAR™ these pixels are referred to as Permanent Scatterers (PS). The result is the identification of a sparse grid of point-like targets on which an atmospheric correction procedure can be performed. Once these errors are removed, a history of motion can be created for each target, allowing the detection of both linear and non-linear motion.

The result is a sparse grid of PS that are color-coded according to their deformation rate and direction of movement. The information available for each PS includes its deformation rate, acceleration, total deformation, elevation, coherence as well as a time series of movement. PSInSAR™ measures ground movement rate with millimeter accuracy.

Appendix 2 contains detailed information on the data processing.

## SqueeSAR™

PS are objects, such as buildings, fences, lampposts, transmission towers, crash barriers, or rock outcrops, that are excellent reflectors of radar microwaves. However, TRE has noticed that many other signals are present in the processed data. These do not produce the same high signal-to-noise ratios of PS but are

nonetheless distinguishable from the background noise. Upon further investigation it was found that the signals are reflected from extensive homogeneous areas where the back-scattered energy is less strong, but statistically consistent. These areas have been called Distributed Scatterers (DS) and correspond to rangeland, pastures, bare earth, debris fields, arid environments, etc. (Figure 17).

The SqueeSAR™ algorithm was developed to process the signals reflected from these areas. As SqueeSAR™ incorporates PSInSAR™ no information is lost and movement measurement accuracy is unchanged.

SqueeSAR™ also produces improvements in the quality of the displacement time series. The homogeneous areas that produce DS normally comprise several pixels. The single time series attributed to each DS is estimated by averaging the time series of all pixels within the DS, effectively reducing noise in the data.

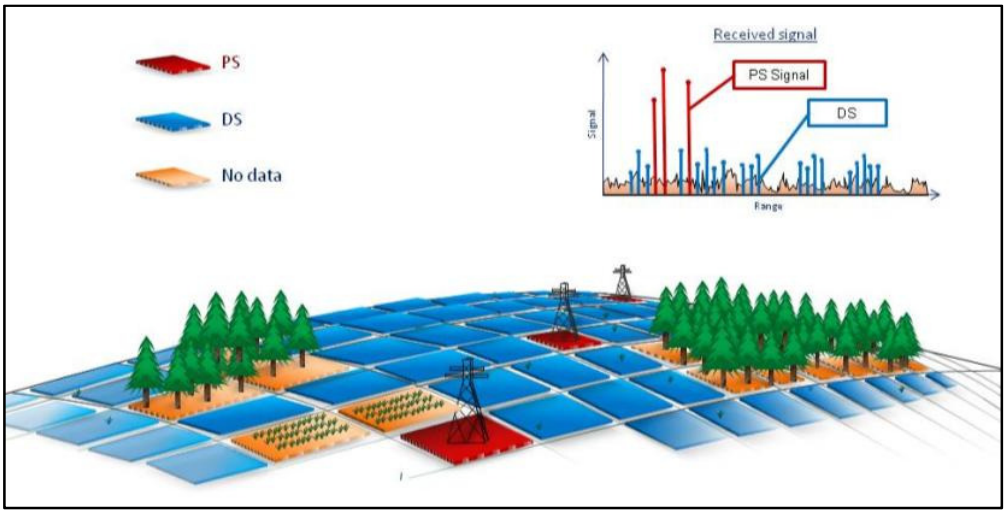


**Figure 17. Illustration of the identification of Permanent Scatterers (PS) and Distributed Scatterers (DS) by the SqueeSAR™ algorithm.**

# Appendix 2: Data processing

## Methodology

The identification of PS and DS in a series of radar images comprises a sequence of steps.

First, all radar data archives are screened to determine the most suitable source of raw data for the particular area of interest and to select all the high quality images within the chosen dataset.

As the signal echo from a single point target contains many returning radar pulses it appears defocused in a synthetic aperture radar (SAR) raw image. The first processing step is therefore to focus all the received energy from a target in one pixel. The images are then precisely aligned to each other, or co-registered, and analysed for their suitability for interferometry. The parameters that are analyzed are the normal baseline and the temporal distribution of the images.

There then follows a number of statistical analyses on the phase and amplitude characteristics of the backscattered radar signal that return to the satellite. If a concentrated number of signals reflect off a particular feature within a pixel and backscatter to the satellite, the feature is referred to as a 'scatterer'. When the same scatterer appears in all, or most, of a data set of SAR images of a particular location, then the scatterer is deemed to be 'permanent'.

At this stage it is possible to identify a subset of pixels, referred to as Permanent Scatterer Candidates (PSC), that are used to estimate the impact on signal phase of ionospheric, tropospheric and atmospheric effects, as well as possible orbit errors.

Once the signal phase has been corrected for these effects, any remaining changes in signal phase directly reflect ground movement.

## Master Image Selection

SqueeSAR™ requires that one image (or scene) in each dataset has to become both a geometric and temporal reference to which all the other images are then related. This image is referred to as the master image and those that remain are slave images.

The master image should be chosen according to the following criteria:

- it minimises the spread of normal baseline values for the slave images;
- similarly, it minimises the temporal baseline values between the master and each slave image; and
- it minimises the effects of signal noise arising from changes in vegetation cover and/or small changes in the look angle of the satellite from one scene to another.

## Signal Phase and Amplitude Analysis

### General

Each pixel of a SAR image contains information on the amplitude of signals that are backscattered toward the satellite, as well as on the signal phase. The amplitude is a measure of the amount of the radar pulse energy reflected, while the phase is related to the length of the path of the electromagnetic wave, from the platform to the ground and back again.

Analyses of both amplitude and phase of the SAR image provide an indication of the stability of each pixel, over time, whereby it is possible to identify those pixels that are most likely to behave as Permanent Scatterers. Statistical methods are used extensively in this process.

Among the different statistical parameters that can be computed two are of particular interest: the Phase Stability Index (PSI), obtained from the phases of the images within the dataset, and the Multi Image Reflectivity (MIR) map, derived from the amplitude values of the available acquisitions.

**Radar Phase and Coherence**

The phase stability is strongly linked to the concept of coherence. Pixels that consistently display high phase stability are said to be coherent. Coherence is measured by an index which ranges from 0 to 1. When a pixel is completely coherent, it will have a coherence value of 1. Correspondingly, if a pixel has a low phase stability, its coherence index will be 0. In general, interferometry is successful when the coherence index lies between 0.5 and 1.0.

**Radar Amplitude and Multi-Image Reflectivity**

The amplitude of a pixel within a SAR image is the aggregate of the backscattered energy toward the satellite from within the pixel's equivalent land area. This equivalent land area is referred to as the radar resolution, and in the case of the data acquired for this project from the ERS and ENVISAT satellites, it measures approximately 20 by 4 meters. The data acquired from the RADARSAT-1 satellite for this project has a radar resolution of 20 by 5 meters.

If a target has experienced significant change in its surface characteristics it will exhibit variation in its reflectivity (electromagnetic response) between two acquisitions. In such circumstances, the possibility of detecting movement by means of SAR interferometry is seriously compromised as the signal phase difference now contains not only the contribution due to displacement, but also that due to changes in the reflectivity of the target. This prevents, in the worst case, the obtaining of any useful information on ground movement.

Accordingly, it is necessary to look into the amplitude values of all the images in the dataset, in order to understand exactly what was seen by the satellite at the time of each acquisition.

Another artefact linked to amplitude is known as speckle. Speckle is random noise that appears as a grainy salt and pepper texture in an amplitude image. This is caused by random interference from the multiple scattering returns that occur within each resolution cell. Speckle has an adverse impact on the quality and usefulness of SAR images. However, the higher the number of images taken of the same area at different times or from slightly different 'look' angles, the easier it is to reduce speckle. This increases the quality and level of details of the amplitude image, enabling it to be used as a background layer for observing the presence of PS results.

The Multi Image Reflectivity (MIR) map is the means by which speckle reduction is accomplished. Averaging a number of images tends to negate the random amplitude variability, leaving the uniform amplitude level unchanged.

MIR images derived from the ERS and RADARSAT-1 image archives over this area are shown in Figure 18 and Figure 19.

It should be emphasized that the information in the MIR map is the reflectivity of each pixel, i.e. the ability to backscatter the incident wave toward the satellite. Flat surfaces (roads, highway, rivers, lakes) act like a mirror, meaning that if their orientation is not exactly perpendicular to the incident wave negligible energy is reflected back to the sensor; they appear dark in the image. On the other hand, because of their irregular physical shape, metal structures or buildings reflect a significant portion of the incident signal back to the radar, resulting in very bright pixels in the MIR map.

**Figure 18. Multi-image reflectivity map of the ERS descending dataset extending over the San Bruno area.**

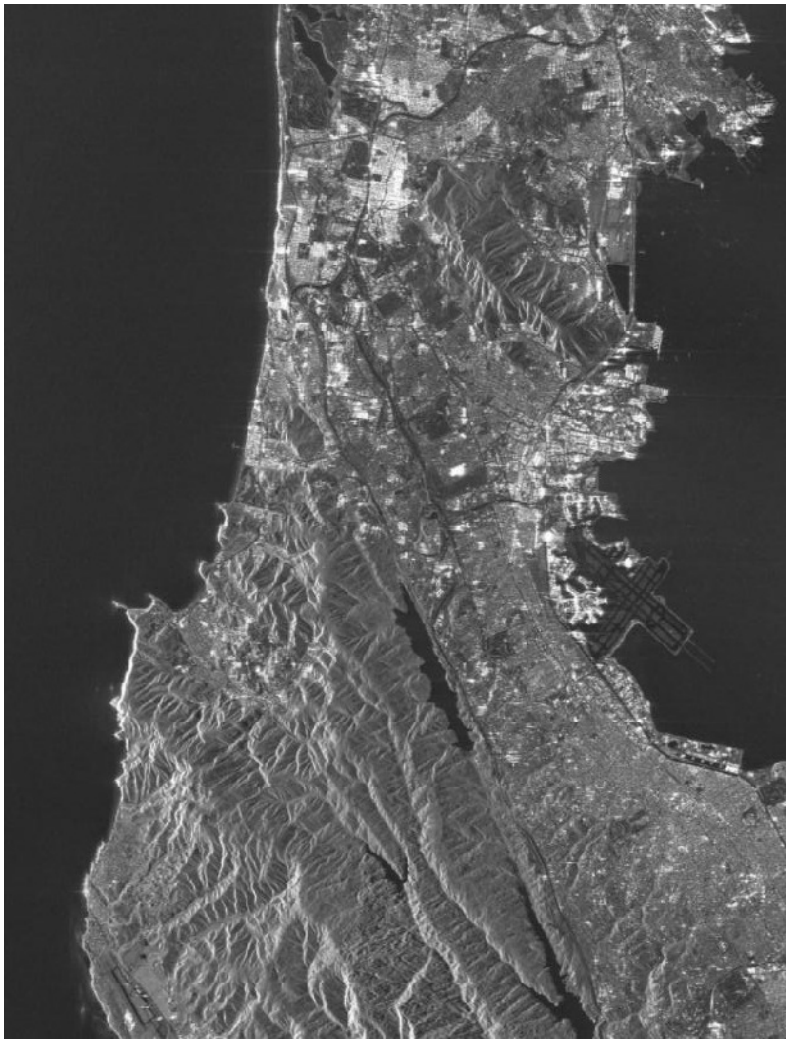

**Figure 19. Multi-image reflectivity map of the RADARSAT-1 ascending dataset extending over the San Bruno area.**

## Interferograms

After the statistical analyses of the SAR images have been completed, a set of differential interferograms is generated. This entails subtracting the phase of each slave image from the phase of the master image. In doing so, the difference in signal path length between the two images is calculated. This difference is related to possible ground motion.

In any SAR image, there are embedded topographic distortions that arise during image acquisition. These are removed using a reference Digital Elevation Model (DEM), leaving ground movement and the signal phase distortions arising from atmospheric effects as the only embedded variables.

The differential interferograms represent the starting point for applying the PSInSAR™ approach.

## Estimation of the atmospheric effects

When a radar signal enters and exits a moisture-bearing layer in the atmosphere, its wavelength can be affected, introducing potential errors into the signal path length. The removal of atmospheric impacts is fundamental for increasing the precision of ground movement measurement.

A sub-set of pixels, usually corresponding to buildings, lampposts, antennas, small structures and exposed rocks, is chosen from among those that have high PSI values. These are referred to as PS Candidates (PSC). PSC density is, of course, higher in towns and cities rather than in forests and vegetated areas. However, it is often possible to obtain good PSC density in rural areas.

For each image, the atmospheric impacts are estimated at each PSC location. The process is statistically based and benefits in accuracy by the greater the number of available images for the analysis. By comparing the atmospheric contribution on neighbouring pixels that would be experiencing the same atmospheric conditions, the atmospheric contribution can be reconstructed over the whole image.

The processed dataset allows identification of a PSC cluster dense enough to identify and extract the atmospheric contribution over the entire area of interest.

## Post-processing

In this stage the processed data undergoes a thorough quality control following ISO 9001:2000 guidelines. The PS data is checked for anomalies, aligned on an optical image layer, and the final report is prepared.

# Appendix 3: Abbreviations and Acronyms

| | |
|---|---|
| APS | Atmospheric Phase Screen |
| ASAR | Advanced Synthetic Aperture Radar |
| AOI | Area Of Interest |
| DEM | Digital Elevation Model |
| DInSAR | Differential Interferometric SAR |
| DS | Distributed Scatterer(s) |
| ERS | Earth Resources Satellite |
| ESA | European Space Agency |
| GCP | Ground Control Point |
| GIS | Geographic Information System |
| GPS | Global Positioning System |
| InSAR | Interferometric SAR |
| LOS | Line Of Sight |
| POLIMI | Politecnico di Milano |
| PS | Permanent Scatterer(s) |
| PSI | Phase Stability Index |
| PSInSAR™ | Permanent Scatterers SAR Interferometry is a world-wide POLIMI Trademark |
| SAR | Synthetic Aperture Radar |
| SNR | Signal to Noise Ratio |
| SqueeSAR™ | The most recent InSAR algorithm patented by TRE |
| TRE | Comprehensive term for Tele-Rilevamento Europa and TRE Canada |
| TS | (Permanent Scatterer and Distributed Scatterer Displacement) Time Series |

TRE®

*Sensing the Planet*

**TRE Canada Inc.**
**409 Granville Street, Suite 550**
**Vancouver, B.C., V6B 1T2**
**Canada**

**Tel. 604 331-2512**
**www.trecanada.com**